Proceedings of the 17th World Congress
The International Federation of Automatic Control
Seoul, Korea, July 6-11, 2008

Direct and Indirect Stable Adaptive Control for Suspension Systems with MR Damper

Itthisek Nilkhamhang * **Tomoaki Mori** * **Akira Sano** *

* *Department of System Design Engineering, Keio University, Yokohama, Japan (Tel : +81-45-566-1730; E-mail: art@contr.sd.keio.ac.jp, mori@contr.sd.keio.ac.jp, sano@sd.keio.ac.jp).*

Abstract: The paper is concerned with stable adaptive schemes for semi-active control of suspension systems, which can deal with uncertainties in a nonlinear model of MR damper. To compensate for unknown nonlinear hysteresis dynamics of the MR damper, an adaptive inverse controller is implemented by indirect and direct methods. In the indirect method, on-line identification of a forward model of MR damper is executed. The direct method updates the inverse controller directly. Then a linear control scheme is designed and applied to the nonlinearly compensated system to give the desired damping force by taking into account the passivity of the MR damper. The effectiveness of the proposed adaptive semiactive control scheme is validated and the stability of the obtained total adaptive system is analyzed.

1. INTRODUCTION

Magnetorheological (MR) damper is a promising semi-active device in areas of vibration isolation for suspension systems and civil structures. The viscosity of MR fluid is controllable depending on input voltage or current. Since the MR damper inherently has uncertain nonlinear hysteresis dynamics, its modeling is an important issue in realization of semi-active vibration isolation control. In the present paper we give a stable robust adaptive inverse controller which can compensate for uncertain nonlinear hysteresis dynamics of the MR damper. The robust LQ controller is also employed to generate desirable damper force to attain vibration isolation of suspension system. The main purpose of the paper is to analyze the stability of the total system consisting of the adaptive inverse controller and robust LQ controller.

The adaptive inverse controller is realized by identifying a forward model of the MR damper or by directly adjusting the inverse model of MR damper without identification of the forward model. Many efforts have been devoted to construction of forward models of MR damper from static and dynamic points of view (Spencer et al. [1997], Yang [2001], Choi et al. [1998], Pan et al. [2000]). The Bouc-Wen model and its variations are typical models which can express the hysteresis dynamics explicitly (Spencer et al. [1997], Yang [2001]), and Hammerstein class of nonlinear model was also investigated (Song et al. [2005]). However, they include too many parameters in nonlinear forms to identify in an on-line manner. Alternative modeling is based on the LuGre friction model (René et al. [2005]) which was originally developed to describe nonlinear friction phenomena (Canudas et al. [1995]). It has rather simple structure and the number of model parameters can also be reduced, however, it is not adequate for real-time design of an inverse controller by using the obtained forward model. We have obtained the new MR damper model by modifying the LuGre model and given an analytical method for adaptive inverse controller design (Sakai et al. [2003], Terasawa et al. [2004]). However, since some adjusted parameters appear in the denominator of the adaptive inverse controller, the stability of the total system is only assured in restricted conditions. In this paper, we also give an adaptive scheme to directly adjust the inverse controller with linearly parameterized form without using the forward model.

The LQ controller can give the desired damping force to match the seat dynamics to a desirable reference dynamics. The previous works based on deterministic control schemes were by the clipped-optimal control (Dyke et al. [1996], Lai et al. [2002]), LQ control (Zhang et al. [2006]), gain-scheduled control (Nishimura et al. [2002]), and H_∞ control (Shimizu et al. [1999], Du et al. [2005], Sakai et al. [2006]), where any adaptive schemes were not employed. One of the main purposes of the paper is to give the LQ control scheme taking into account the dissipativity of the MR damper and to clarify the stability condition of the total semi-active control system considering interaction between the adaptive inverse controller and LQ controller. Finally the validity of the proposed control scheme is discussed in numerical simulation.

2. SEMI-ACTIVE SUSPENSION SYSTEM

Fig.1 illustrates a simple suspension system installed with MR damper between the car chassis and the wheel assembly. The dynamic equation is expressed by

$$M_s\ddot{x}_s + C_s(\dot{x}_s - \dot{x}_u) + K_s(x_s - x_u) = -F_{MR} \quad (1)$$

$$M_u\ddot{x}_u + C_s(\dot{x}_u - \dot{x}_s) + K_s(x_u - x_s) + K_t(x_u - x_r) = F_{MR} \quad (2)$$

where M_s is the sprung mass, which represents the car chassis, M_u is the unsprung mass, which represents the wheel assembly; C_s and K_s are damping and stiffness of the uncontrolled suspension system, respectively; K_t serves to model the compressibility of the pneumatic tyre. x_s and x_u are the displacements of the sprung and unsprung mass, respectively; x_r is the road displacement input; F_{MR} is the damping force supplied by the MR damper. This can be represented in the state-space form as

$$\dot{\boldsymbol{x}}_p = \boldsymbol{A}\boldsymbol{x}_p + \boldsymbol{b}F_{MR} + \boldsymbol{e}\dot{x}_r \quad (3)$$

where

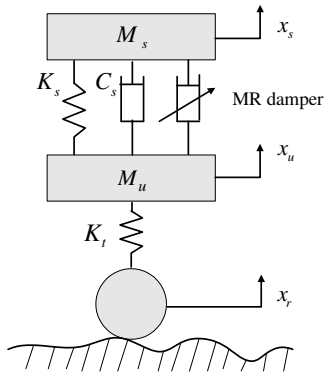

Fig. 1. Suspension system with MR damper

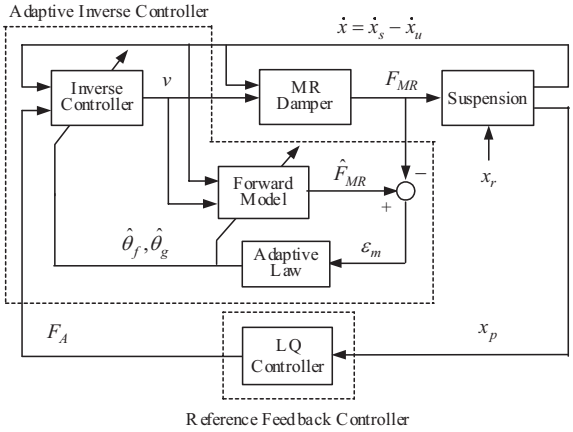

Fig. 2. Proposed indirect adaptive semiactive control scheme based on *forward* modeling

$$\boldsymbol{x}_p = [x_s - x_u \;\; x_u - x_r \;\; \dot{x}_s \;\; \dot{x}_u]^T$$

$$\boldsymbol{A} = \begin{bmatrix} 0 & 0 & 1 & -1 \\ 0 & 0 & 0 & 1 \\ -K_s/M_s & 0 & -C_s/M_s & C_s/M_s \\ K_s/M_u & -K_t/M_u & C_s/M_u & -C_s/M_u \end{bmatrix}$$

$$\boldsymbol{b} = [0 \;\; 0 \;\; -1/M_s \;\; 1/M_u]^T$$

$$\boldsymbol{e} = [0 \;\; -1 \;\; 0 \;\; 0]^T$$

Fig.2 and Fig.3 show schematic diagrams of the proposed adaptive semiactive control for the suspension system. The adaptive algorithm consists of two controllers: the first is a linear quadratic (LQ) controller with full-state feedback that generates a command damping force F_A, when the parameters of the suspension system are known; the second is an adaptive inverse controller which can give required input voltage v to MR damper so that the damping force F_{MR} is equal to F_A. If the adaptive inverse controller is designed so that the linearization from F_A to F_{MR} can be attained, that is, $F_A = F_{MR}$, we can realize almost active control performance. For construction of the inverse controller, the forward model of MR damper is identified and then the input voltage to MR damper is calculated as shown in Fig.2. Fig.3 gives an alternative scheme in which the inverse controller is directly updated without identification of MR damper. Since the MR damper is actually a nonlinear semi-active device, it is difficult to make it work as an active device, and it needs very fine and complicated tuning

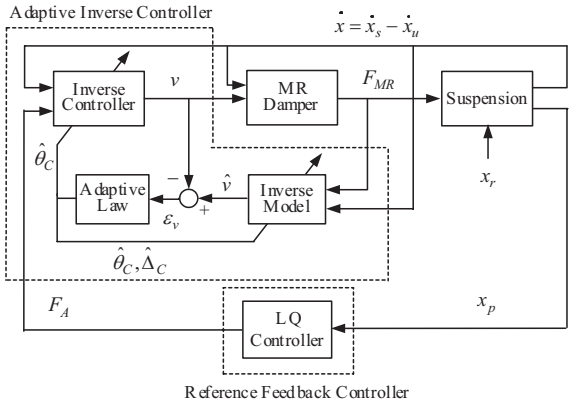

Fig. 3. Proposed direct adaptive semiactive control scheme based on *inverse* modeling

of both the adaptive inverse controller and adaptive reference controller.

3. ROBUST LQ CONTROL WITH DISSIPATIVITY

This paper uses robust LQ control to design the active damping force F_A. The semi-active constraint of the MR damper signifies that $F_{MR} \neq F_A$ and therefore it is necessary to define the following disturbance term

$$\delta_{MR} = F_{MR} - F_A \tag{4}$$

which is assumed to be bounded by

$$\|\delta_{MR}\|_2 \leq \Delta_{MR} \tag{5}$$

Restating (3) in terms of F_A and δ_{MR},

$$\dot{\boldsymbol{x}}_p = \boldsymbol{A}\boldsymbol{x}_p + \boldsymbol{b}F_A + \boldsymbol{b}\delta_{MR} + \boldsymbol{e}\dot{x}_r \tag{6}$$

The robust control objective becomes

$$J_\infty = \sup_{\delta_{MR} \in L_2} \frac{\|z\|_2}{\|\delta_{MR}\|_2} < \gamma \tag{7}$$

where

$$z = \begin{bmatrix} \left(\boldsymbol{Q} - r^{-1}\boldsymbol{s}\boldsymbol{s}^T\right)^{\frac{1}{2}} & \boldsymbol{0} \\ r^{-\frac{1}{2}}\boldsymbol{s}^T & r^{\frac{1}{2}} \end{bmatrix} \begin{bmatrix} \boldsymbol{x}_p \\ F_A \end{bmatrix} \tag{8}$$

where $\boldsymbol{Q} = q\boldsymbol{I}$ and $\boldsymbol{s} = \begin{bmatrix} \boldsymbol{0}^T & s_1 & s_2 \end{bmatrix}^T$, while $q > 0$ and $r > 0$. Therefore

$$\begin{aligned} \|z\|_2 &= \int_0^\infty \begin{bmatrix} \boldsymbol{x}_p^T & F_A \end{bmatrix} \begin{bmatrix} \boldsymbol{Q} & \boldsymbol{s} \\ \boldsymbol{s}^T & r \end{bmatrix} \begin{bmatrix} \boldsymbol{x}_p \\ F_A \end{bmatrix} dt \\ &= \int_0^\infty \left(\boldsymbol{x}_p^T \boldsymbol{Q}\boldsymbol{x}_p + 2\boldsymbol{x}_p^T \boldsymbol{s}F_A + rF_A^2\right) dt \end{aligned} \tag{9}$$

Assuming that the road perturbation $\dot{x}_r$ is a random signal with zero mean, the active control force considering the disspativity is given by

$$F_A = -\boldsymbol{k}^T \boldsymbol{x}_p \tag{10}$$

$$\boldsymbol{k} = \frac{\boldsymbol{P}\boldsymbol{b} + \boldsymbol{s}}{r} \tag{11}$$

and $\boldsymbol{P}$ is the solution of the corresponding Riccati equation:

$$\boldsymbol{Q} + \boldsymbol{P}\boldsymbol{A} + \boldsymbol{A}^T\boldsymbol{P} - \boldsymbol{P}\boldsymbol{b}\left(1 - \gamma^{-2}\right)\boldsymbol{b}^T\boldsymbol{P} = \boldsymbol{0} \tag{12}$$

If all of the states are not available, the observer can be designed from the sensor data, for instance $x_s - x_u$ and $\ddot{x}_s$, and an output controller is implemented.

4. ADAPTIVE INVERSE CONTROL SCHEMES

4.1 Indirect Adaptive Control via Forward Modeling

MR damper is a semi-active device in which the viscosity of the fluid is controllable by the input voltage or current. A variety of approaches have been taken to modeling of the nonlinear hysteresis behavior of the MR damper. Compared to the Bouc-Wen model (Spencer et al. [1997],Yang [2001]), the LuGre model has simpler structure and smaller number of parameters needed for expression of its behavior (René et al. [2005]). We have also modified the LuGre model so that a necessary input voltage can be analytically calculated to produce the specified command damping force F_A (Sakai et al. [2003]).

The damping force F_{MR} is expressed by

$$F_{MR} = \sigma_a z + \sigma_0 z v + \sigma_1 \dot{z} + \sigma_2 \dot{x} + \sigma_b \dot{x} v, \tag{13}$$

$$\dot{z} = \dot{x} - a_0 |\dot{x}| z \tag{14}$$

$$x = x_s - x_u \tag{15}$$

where z is an internal state variable [m], x is the relative displacement between the car chassis and the wheel assembly [m], σ_0 stiffness of z influenced by v [N/(m·V)], σ_1 damping coefficient of z [N·s/m], σ_2 viscous damping coefficient [N·s/m], σ_a stiffness of z [N/m], σ_b viscous damping coefficient influenced by v [N·s/(m·V)], and a_0 constant value [V/N]. The model was validated in experimental data (Terasawa et al. [2004]).

Substituting (14) into (13) gives the nonlinear input-output relation as

$$\begin{aligned} F_{MR} &= \sigma_a z + \sigma_0 z v - \sigma_1 a_0 |\dot{x}| z + (\sigma_1 + \sigma_2)\dot{x} + \sigma_b \dot{x} v \\ &= \boldsymbol{\theta}_f^T \boldsymbol{\varphi}_f + \boldsymbol{\theta}_g^T \boldsymbol{\varphi}_g v \end{aligned} \tag{16}$$

where $\boldsymbol{\theta}_f = (\sigma_a,\ \sigma_1 a_0,\ \sigma_1 + \sigma_2)^T$ and $\boldsymbol{\varphi}_f = (z,\ -|\dot{x}|z,\ \dot{x})^T$, $\boldsymbol{\theta}_g = (\sigma_0,\ \sigma_b)^T$ and $\boldsymbol{\varphi}_g = (z,\ \dot{x})^T$. Since the internal state z of the MR damper model cannot be measured, the regressor vectors should be replaced with their estimates as

$$\hat{\boldsymbol{\varphi}}_f = [\hat{z}\ -|\dot{x}|\hat{z}\ \dot{x}]^T \tag{17}$$

$$\hat{\boldsymbol{\varphi}}_g = [\hat{z}\ \dot{x}]^T \tag{18}$$

where the estimate $\hat{z}$ is given later by using the updated model parameters. The output of the identification model is now described as

$$\hat{F}_{MR} = \hat{\boldsymbol{\theta}}_f^T \hat{\boldsymbol{\varphi}}_f + \hat{\boldsymbol{\theta}}_g^T \hat{\boldsymbol{\varphi}}_g v \tag{19}$$

where $\hat{\boldsymbol{\theta}}_f$ and $\hat{\boldsymbol{\theta}}_g$ are the parameter estimates. By using the damping force estimation error defined by $\varepsilon_m \equiv \hat{F}_{MR} - F_{MR}$, and the identified parameter $\hat{a}_0$, the estimate $\hat{z}$ of the internal state can be calculated as

$$\dot{\hat{z}} = \dot{x} - \hat{a}_0 |\dot{x}| \hat{z} - l\varepsilon_m, \tag{20}$$

where l is an observer gain such that $0 \le l \le 1/\hat{\sigma}_{1\max}$, and the upper bound is decided by the stability of the adaptive observer Terasawa et al. [2004]. The adaptive laws for updating the model parameters are given as

$$\dot{\hat{\boldsymbol{\theta}}}_f = -\boldsymbol{\Gamma}_f \hat{\boldsymbol{\varphi}}_f \varepsilon_m - \sigma_f \boldsymbol{\Gamma}_f \hat{\boldsymbol{\theta}}_f \tag{21}$$

$$\dot{\hat{\boldsymbol{\theta}}}_g = -\boldsymbol{\Gamma}_g \hat{\boldsymbol{\varphi}}_g v \varepsilon_m - \sigma_g \boldsymbol{\Gamma}_g \hat{\boldsymbol{\theta}}_g \tag{22}$$

where $\boldsymbol{\Gamma}_f$ and $\boldsymbol{\Gamma}_g$ are positive definite matrices, σ_f and σ_g are positive design constants. Though $\boldsymbol{\Gamma}_f$ and $\boldsymbol{\Gamma}_g$ may vary with time, it is defined by this paper as constant for practical implementation.

The role of the adaptive inverse controller shown in Fig.2 is to decide the control input voltage v to the MR damper so that the actual damping force F_{MR} approaches the specified command damping force F_A, even in the presence of uncertainty in the MR damper model. The input voltage giving F_A can be analytically calculated from the identified forward model of MR damper. Actually using the identified model parameters, the input voltage v is obtained from (16) as

$$\rho = \hat{\boldsymbol{\theta}}_g^T \hat{\boldsymbol{\varphi}}_g \tag{23}$$

$$d_\rho = \begin{cases} \rho & \text{for } \rho < -\delta,\ \delta < \rho \\ \delta\,\mathrm{sgn}(\rho) & \text{for } -\delta \le \rho \le \delta \end{cases} \tag{24}$$

$$v_A = \frac{F_A - \hat{\boldsymbol{\theta}}_f^T \hat{\boldsymbol{\varphi}}_f - l\varepsilon_m}{d_\rho} \tag{25}$$

$$v = sat(v_A), \quad 0 \le v \le V_{\max} \tag{26}$$

where F_A is the optimal control force as determined by the LQ controller. v_A is assumed to be fixed near $\rho = 0$ to avoid division by zero. Due to these saturation effects, the semi-active force F_{MR} may not fully match the active optimal control force F_A. Stability analysis results are similar to the case of indirect adaptive control via inverse modeling, which is presented in the appendix.

4.2 Direct Adaptive Control via Inverse Modeling

In the previous section, the inverse controller is obtained analytically from the estimated parameters of the forward model of MR damper. However, as expressed in (25), some adjustable parameters appear in the denominator of the inverse controller and so zero-division should be avoided. Therefore, we consider a linearly parameterized *inverse* model, as shown in Fig.3. Since the damper force F_{MR} is given as a function of the velocity $\dot{x}$, input voltage v and internal state z as shown in (16), its inverse model for the input voltage v can be expressed as a function of $\dot{x}$, z and F_{MR}. Hence, we consider an inverse model which is expressed by a linearly parameterized polynomial model as:

$$v = \sum_{j=0}^{n} \sum_{i=0}^{m} h_{i+(m+1)k+1} |\dot{x}|^i |z|^j F_{MR} \mathrm{sgn}(\dot{x}) + \delta_c \tag{27}$$

where the inverse model has two inputs of $\dot{x}$ and F_{MR}, and one output of v. z is an internal state of the MR damper, which can be calculated as given previously by

$$\dot{z} = \dot{x} - a_0 |\dot{x}| z$$

where a nominal value of a_0 is assumed to be known via the forward modeling. δ_c represents the unknown approximation error, which is assumed to be bounded,

$$\sup |\delta_c| \le \Delta_C \tag{28}$$

The unknown bound Δ_C can be made arbitrary small by increasing the order of polynomial approximation. In simulation, an inverse model with $m = 4$ and $n = 1$ is adopted.

The inverse model is also expressed in a vector form as

$$v = \boldsymbol{\theta}_c^T \boldsymbol{\varphi}_c + \delta_c \tag{29}$$

where

$$\boldsymbol{\theta}_c = (h_1,\ h_2,\ \cdots,\ h_{(n+1)(m+1)})^T \tag{30}$$

$$\begin{aligned} \boldsymbol{\varphi}_c = (&F_{MR}\,\mathrm{sgn}(\dot{x}),\ |\dot{x}|F_{MR}\,\mathrm{sgn}(\dot{x}),\ \cdots,\ |z|F_{MR}\,\mathrm{sgn}(\dot{x}) \\ &|\dot{x}||z|F_{MR}\,\mathrm{sgn}(\dot{x}),\ \cdots, |\dot{x}|^m |z|^n F_{MR}\,\mathrm{sgn}(\dot{x}))^T \end{aligned} \tag{31}$$

Then the identified model is expressed as

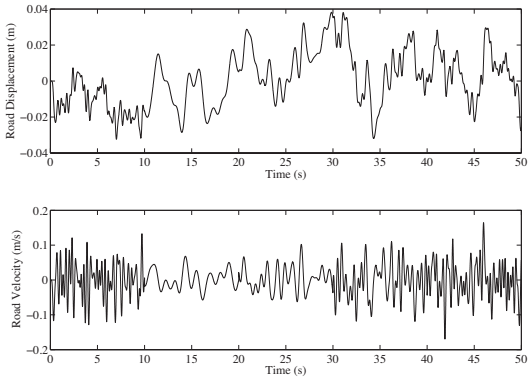

Fig. 4. Road excitation, displacement x_r and velocity $\dot{x}_r$.

$$\hat{v} = \hat{\boldsymbol{\theta}}_c^T \boldsymbol{\varphi}_c + \mu \tag{32}$$

where the identification error ε_v is defined as

$$\varepsilon_v = \hat{v} - v \tag{33}$$

and μ is a robustifying term given as

$$\mu = \hat{\Delta}_c \eta_c \tanh((a+bt)\varepsilon_v) \tag{34}$$

$\eta_c > 1$ and $a, b > 0$. The adaptive parameters $\hat{\boldsymbol{\theta}}_c$ and $\hat{\Delta}_v$ are adjusted in an on-line manner so as to minimize the identification error according to the following adaptive laws

$$\dot{\hat{\boldsymbol{\theta}}}_c = -\boldsymbol{\Gamma}_c \boldsymbol{\varphi}_c \varepsilon_v - \sigma_c \boldsymbol{\Gamma}_c \hat{\boldsymbol{\theta}}_c \tag{35}$$

$$\dot{\hat{\Delta}}_c = \gamma_{\Delta_c} |\varepsilon_v| - \sigma_{\Delta_c} \gamma_{\Delta_c} \hat{\Delta}_c \tag{36}$$

where $\boldsymbol{\Gamma}_c$ is a positive definite matrix, γ_{Δ_c}, σ_c and σ_{Δ_c} are positive design constants. For practical implementation, $\boldsymbol{\Gamma}_c$ is chosen constant.

Fig.3 describes the indirect adaptive damper control via inverse modeling. The control input voltage v is given as

$$v_A = \hat{\boldsymbol{\theta}}_c^T \boldsymbol{\varphi}_A \tag{37}$$

$$v = \begin{cases} 0 & \text{for } v_A \le 0 \\ v_A & \text{for } 0 < v_A \le V_{\max} \\ V_{\max} & \text{for } V_{\max} < v_A \end{cases} \tag{38}$$

where

$$\boldsymbol{\varphi}_A = (F_A \operatorname{sgn}(\dot{x}),\ |\dot{x}|F_A \operatorname{sgn}(\dot{x}),\ \cdots,\ |z|F_A \operatorname{sgn}(\dot{x}),\ |\dot{x}||z|F_A \operatorname{sgn}(\dot{x}),\ \cdots, |\dot{x}|^m |z|^n F_A \operatorname{sgn}(\dot{x}))^T \tag{39}$$

Again due to the semi-active nature of the MR damper, F_{MR} may not fully match the active optimal control force F_A. Stability analysis and results are provided in the appendix.

5. SIMULATION RESULTS

Consider a suspension system shown in Fig. 1, where the parameters are set as $M_s = 504.5$ [kg], $M_u = 62$ [kg], $C_s = 400$ [Ns/m], $K_s = 1.31 \times 10^4$ [N/m] and $K_t = 2.52 \times 10^5$ [N/m]. The parameters of the MR damper are specified as: $\sigma_0 = 4.0 \times 10^4$ [N/mV], $\sigma_1 = 2.0 \times 10^2$ [Ns/m], $\sigma_2 = 1.0 \times 10^2$ [Ns/m], $\sigma_a = 1.5 \times 10^4$ [N/m], $\sigma_b = 2.5 \times 10^3$ [Ns/(mV)], $a_0 = 1.9 \times 10^2$, which are all unknown. An upper limit of input voltage to the MR damper is set at 2.5[V], so v varies between 0 to 2.5[V]. The base of the dynamic system in Fig. 1 is excited by the road surface, which is given by a random signal sequence with a frequency range of 0-3.5 Hz. To analyze the effectiveness of each control schemes for various frequency ranges, the road excitation was designed so that the bandwidth increases every ten seconds from 1Hz, 1.5Hz, 2.5Hz to 3.5Hz. The initial period

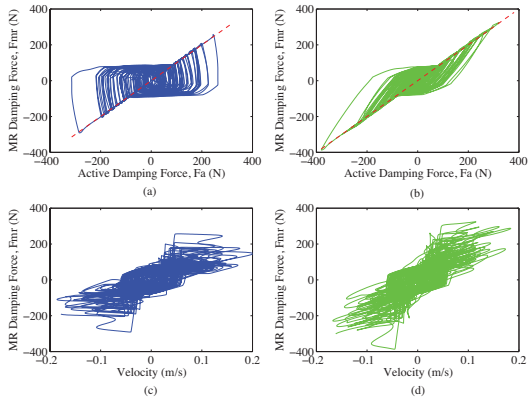

Fig. 5. Comparison of F_A and F_{MR} for (a,c) non-dissipative LQ, and (b,d) dissipative LQ.

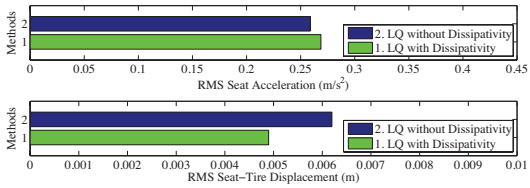

Fig. 6. RMS seat acceleration and RMS seat-tire displacement for non-dissipative and dissipative LQ.

of ten seconds has a bandwidth of 3.5Hz to allow for parameter convergences of the adaptive schemes. The displacement and velocity profile of the road excitation is shown in Figure 4. The following schemes are compared: (1) Passive low damping with 0 [V] fixed, (2) Passive high damping with 2.5 [V] fixed, (3) Active LQ-based scheme, (4) Forward modeling based scheme (Proposed), and (5) Inverse modeling based scheme (Proposed).

First, the role of the dissipativity term in the robust LQ design is demonstrated. This study considered the case when $\boldsymbol{s} = \mathbf{0}$ and when $\boldsymbol{s} = \begin{bmatrix} 0 & 4 \times 10^3 \end{bmatrix}^T$. Figure 5 shows a comparison of the active damping force F_A and the measured damping force F_{MR} for both the non-dissipative and dissipative LQ controllers. The dissipativity term $\boldsymbol{s}$ serves to prevent the active control action from behaving too aggressively, thus allowing the MR damper a greater chance to match the active damping force. This is reflected in Figure 6, where the dissipative LQ controller produces slightly higher RMS acceleration than the non-dissipative LQ controller, due to its less aggressive actions.

Next, the results of the various control algorithms are presented. The damping results are compared by the following criterions: (1) the RMS seat acceleration in Figure 7, and (2) the RMS positional deflection of the seat and the tire in Figure 8. The results in Figures 7 and 8 can be analyzed as follows. The passive low damping produces a small damping force and therefore is suited for higher level of frequencies. The passive high damping provides the stiffest damping, and performs better during the low frequency ranges. The trade off between low and high damping can clearly be seen as the bandwidth of the road excitation is increased. The active control meanwhile provides the best performance regardless of the level of excitation. The semi-active forward and inverse modeling schemes also perform better overall than the fixed damping, as it is able to adjust the stiffness to account for the road excitation. It is noted that there is a trade-off between acceleration and displacement. The performance criterion should therefore be taken into careful

Table 1. Ride comfort evaluation (ISO 2631).

Frequency Range (Hz)	ISO 2631-1 ($\leq$ 1 hour)	LQ Active	LQ + MR Forward	LQ + MR Inverse
0-1	0.8000	0.1140	0.1705	0.2221
0-1.5	0.6400	0.1936	0.2781	0.3493
0-2.5	0.5120	0.2492	0.3291	0.4385
0-3.5	0.4200	0.2346	0.2874	0.4001

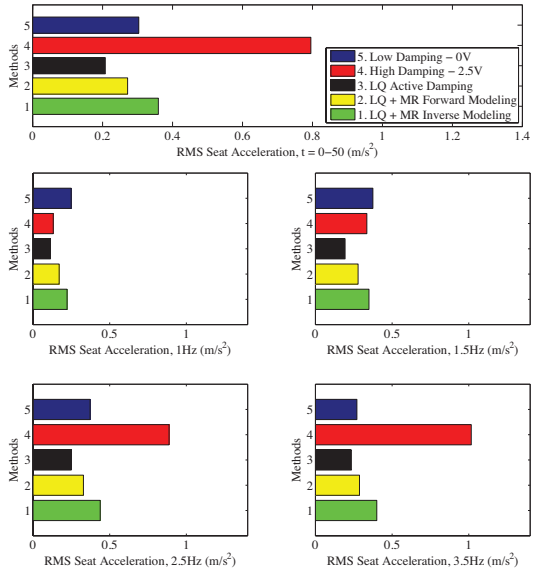

Fig. 7. Comparison of RMS seat acceleration for the entire simulation, and divided into frequency ranges.

consideration during design of the LQ controller. The convergence of the feedforward modeling parameters are shown in Figure 9. A comparison of the active and semi-active damping force is given in Figures 10 and 11.

The evaluation of ride comfort is conducted by comparing the RMS seat acceleration results with the permissible acceleration as specified by ISO 2631. The amount of RMS acceleration that a human being can sustain while remaining comfortable is a function of vibration time and frequency of excitation. For a ride duration of 1 hour, ISO 2631 specifies these values as given in Table 1. By comparing with the results for each methods, it is noted that all values fall within the permissible range, except for high damping at 2.5 and 3.5Hz excitation, thus ensuring that the proposed control methods are able to guarantee ride comfort to the human occupants.

6. CONCLUSION

The three adaptive semi-active suspension control schemes were presented. They consist of adaptive inverse controller which compensates for nonlinear hysteresis dynamics of MR damper, and the LQ controller. Stability conditions of the total semiactive control system has also been clarified, and the effectiveness of the proposed schemes has been validated in simulations.

REFERENCES

C. Canudas, H. Olsson K. J. Åström and P. Lischinsky, A new model for control of systems with friction. *IEEE Trans. Automatic Control*, 40-3, pages 419–425, 1995.

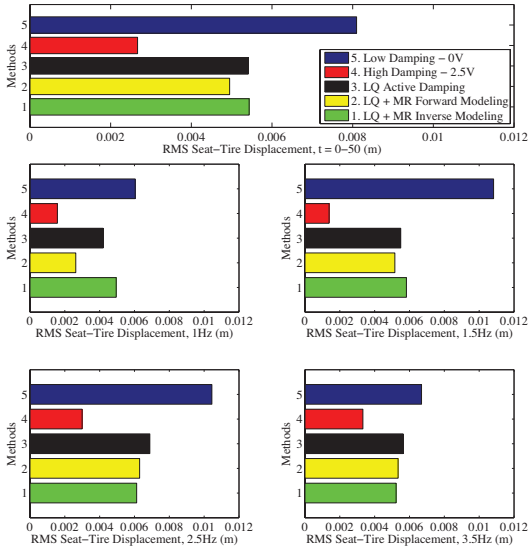

Fig. 8. Comparison of RMS seat-tire displacement for the entire simulation, and divided into different frequency ranges.

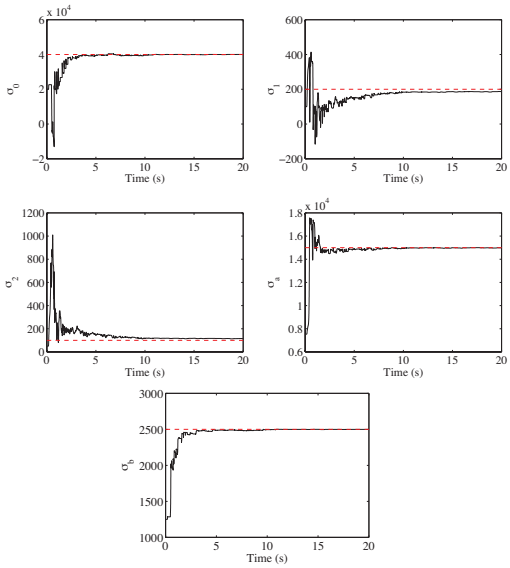

Fig. 9. Convergence of MR parameter estimates for LQ control with forward modeling.

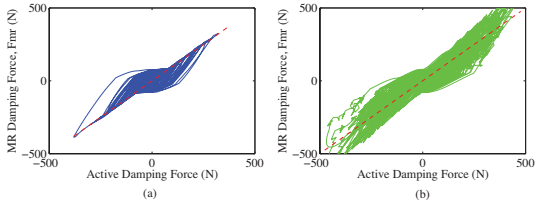

Fig. 10. Comparison of F_A and F_{MR} for (a) LQ with forward modeling and (b) LQ with inverse modeling.

C. C. Chang and L. Zhou, Neural network emulation of inverse dynamics for a magnetorheological damper. *ASCE J. Structural Engineering*, 128-2, pages 231–239, 2002.

S. B. Choi and S. K. Lee, A hysteresis model for the field-dependent damping force of a magnetorheological damper. *J. of Sound and Vibration*, 245-2, pages 375–383, 1998.

H.P. Du, K.Y. Szeb and J. Lam, Semi-active H_∞ control of vehicle suspension with magneto-rheological dampers. *J.*

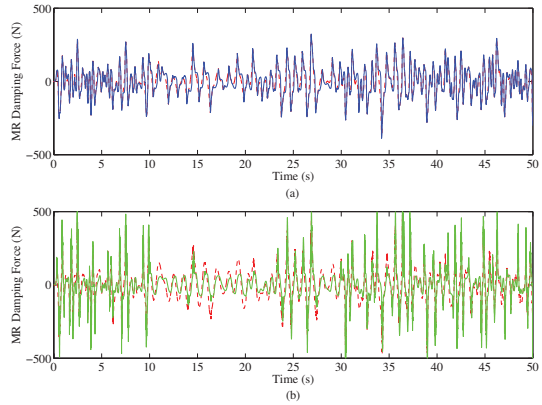

Fig. 11. Plot of F_A (red, dashed) and F_{MR} versus time for (a) LQ with forward modeling and (blue, solid) (b) LQ with inverse modeling (green, solid).

Sound and Vibration, 283, pages 981–996, 2005.

S. J. Dyke, B. F. Spencer Jr. M. K. Sain and J. D. Carlson, Modeling and control of magnetorheological dampers for seismic response reduction. *Smart Materials and Structures* 5, pages 565–575, 1996.

C. Y. Lai and W. H. Liao, Vibration control of a suspension systems via a magnetorheological fluid damper. *Journal of Vibration and Control*, 8, pages 525–547, 2002.

H. Nishimura and R. Kayama, Gain-scheduled control of a semi-active suspension using an MR damper. *Trans. Japan Soc. Mech. Eng.*, 68-676(C), pages 3644–3651, 2002.

G. Pan, H. Matshushita and Y. Honda, Analytical model of a magnetorheological damper and its application to the vibration control. *Proc, IECON*, pages 1850–1855, 2000.

J. René and L. Alvarez, Real time identification of structures with magnetorheological dampers. *Proc. IEEE Conf. Decision and Control*, Las Vegas, USA, pages 1017-1022, 2002.

C. Sakai, H. Ohmori and A. Sano, Modeling of mr damper with hysteresis for adaptive vibration control. *Proc. IEEE Conf. Decision and Control*, Hawaii, USA, 2003.

C. Sakai, T. Terasawa and A. Sano, Adaptive identification of MR damper with application to vibration control. *Trans. SICE*, 42-9, pages 1117–1125, 2006.

E. Shimizu, K. Kubota, M. Sampei and M. Koga, A design of a nonlinear H_∞ state feedback controller for bilinear systems. *Trans. SICE*, 35-9, pages 1155–1161, 1999.

X. Song, M. Ahmadian, S. Southward and L. R. Miller, An adaptive semiactive control algorithm for magnetorheological suspension systems. *Trans. ASME, J. Vib. Acoust.*, 127, pages 493–502, 2005.

B. F. Spencer Jr., S. J. Dyke, M. K. Sain and J. D. Carlson. Phenomenological model of a magnetorheological damper. *ASCE Journal of Engineering Mechanics*, 123-3, pages 230–238, 1997.

T. Terasawa, C. Sakai, H. Ohmori and A. Sano, Adaptive identification of MR damper for vibration control. *Proc. IEEE Conf. Decision and Contr.*, Bahama, 2004.

G. Yang, Large-scale magnetorheological fluid damper for vibration mitigation: modeling, testing and control, The University of Notre Dame, Indiana, 2001.

C. T. Zhang, J. P. Ou and J. Q. Zhang, Parameter optimization and analysis of a vehicle suspension system controlled by magnetorheological fluid damper. *Structural Control and Health Monitoring*, 13, pages 835–896, 2006.

L. Zuo, J. J. E. Slotine and S. A. Nayfeh, Experimental study of a novel adaptive controller for active vibration isolation. *Proc. 2004 American Control Conference*, Boston, USA, 2004.

Appendix A. STABILITY ANALYSIS

A.1 Direct Adaptive Control via Inverse Modeling

This section discusses the stability of indirect adaptive control scheme based upon inverse modeling. The stability analysis of the forward modeling case is similar and is omitted. It is assumed that a_0 is known. From this assumption, the internal state is directly accessible, *i.e.*, $\hat{z} = z$.

Define a candidate of the Lyapunov function as

$$V = \frac{1}{2}\boldsymbol{x}_p^T P \boldsymbol{x}_p + \frac{1}{2}\tilde{\boldsymbol{\theta}}_c^T \boldsymbol{\Gamma}_c^{-1} \tilde{\boldsymbol{\theta}}_c + \frac{1}{2\gamma_{\Delta_c}} \tilde{\Delta}_c^2 \tag{A.1}$$

where $\tilde{\boldsymbol{\theta}}_c = \hat{\boldsymbol{\theta}}_c - \boldsymbol{\theta}_c$ and $\tilde{\Delta}_c = \hat{\Delta}_c - \Delta_c$. Taking the time-derivative of (A.1), using the control law as defined in (37), and applying the adaptive laws (35) and (36) gives

$$\begin{aligned}
\dot{V}_1 &= \frac{1}{2}\boldsymbol{x}_p^T \left(\boldsymbol{P}\boldsymbol{A} + \boldsymbol{A}^T\boldsymbol{P} - 2\boldsymbol{P}\boldsymbol{b}\boldsymbol{k}^T\right)\boldsymbol{x}_p \\
&\quad -\tilde{\boldsymbol{\theta}}_c^T \boldsymbol{\varphi}_c \varepsilon_v + \tilde{\Delta}_c |\varepsilon_v| - \sigma_c \tilde{\boldsymbol{\theta}}_c^T \hat{\boldsymbol{\theta}}_c - \sigma_{\Delta_c} \tilde{\Delta}_c \hat{\Delta}_c \\
&= -\frac{1}{2}\boldsymbol{x}_p^T \left(\boldsymbol{Q} - 2\boldsymbol{s}\boldsymbol{k}^T + r\boldsymbol{k}\boldsymbol{k}^T\right)\boldsymbol{x}_p \\
&\quad -\varepsilon_v^2 + \delta_c \varepsilon_v - \mu \varepsilon_v + \tilde{\Delta}_c |\varepsilon_v| - \sigma_c \tilde{\boldsymbol{\theta}}_c^T \hat{\boldsymbol{\theta}}_c - \sigma_{\Delta_c} \tilde{\Delta}_c \hat{\Delta}_c
\end{aligned} \tag{A.2}$$

We will now use the relationship

$$-\sigma \tilde{\boldsymbol{\theta}}^T \hat{\boldsymbol{\theta}} \le -\frac{\sigma}{2}\tilde{\boldsymbol{\theta}}^T \tilde{\boldsymbol{\theta}} + \frac{\sigma}{2}\boldsymbol{\theta}^T \boldsymbol{\theta} \tag{A.3}$$

along with (28) to obtain

$$\begin{aligned}
\dot{V}_1 \le &-\frac{1}{2}\boldsymbol{x}_p^T \left(\boldsymbol{Q} - 2\boldsymbol{s}\boldsymbol{k}^T + r\boldsymbol{k}\boldsymbol{k}^T\right)\boldsymbol{x}_p \\
&\hat{\Delta}_c \left(1 - \eta_c \tanh((a+bt)|\varepsilon_v|)\right)|\varepsilon_v| \\
&-\frac{\sigma_c}{2}\tilde{\boldsymbol{\theta}}_c^T \tilde{\boldsymbol{\theta}}_c - \frac{\sigma_{\Delta_c}}{2}\tilde{\Delta}_c^2 + \frac{\sigma_c}{2}\boldsymbol{\theta}_c^T \boldsymbol{\theta}_c + \frac{\sigma_{\Delta_c}}{2}\Delta_c^2
\end{aligned} \tag{A.4}$$

Notice that the condition

$$1 - \eta_c \tanh\left((a+bt)|\varepsilon_v|\right) \le 0 \tag{A.5}$$

is satisfied when

$$|\varepsilon_v| \ge \nu_c = \frac{1}{a+bt} \ln\left(\frac{\eta_c + 1}{\eta_c - 1}\right), \quad \eta_c > 1 \tag{A.6}$$

As $t \to \infty$ and $b > 0$, the region defined by ν_c goes to zero, and thus the condition (A.5) is satisfied as $t \to \infty$. It can be shown that there exists $\boldsymbol{M}$ such that

$$\boldsymbol{Q} - 2\boldsymbol{s}\boldsymbol{k}^T + r\boldsymbol{k}\boldsymbol{k}^T = \boldsymbol{M}\boldsymbol{M}^T > 0 \tag{A.7}$$

Therefore,

$$\dot{V}_1 \le -c_1 V_1 + \lambda_1 \tag{A.8}$$

where

$$\begin{aligned}
c_1 &= \min\left\{\frac{\lambda_{\max}(\boldsymbol{M}\boldsymbol{M}^T)}{\lambda_{\min}(\boldsymbol{P})}, \frac{\sigma_c}{\lambda_{\min}(\boldsymbol{\Gamma}_c^{-1})}, \gamma_{\Delta_c}\sigma_{\Delta_c}\right\} \\
\lambda_1 &= \frac{\sigma_c}{2}\boldsymbol{\theta}_c^T \boldsymbol{\theta}_c + \frac{\sigma_{\Delta_c}}{2}\Delta_c^2
\end{aligned} \tag{A.9}$$

As $\lambda_1/c_1 > 0$, (A.8) results in

$$0 \le V_1(t) \le \lambda_1/c_1 + (V_1(0) - \lambda_1/c_1)e^{-c_1 t} \tag{A.10}$$

Therefore all system states $\boldsymbol{x}_p$, error signals $\tilde{\boldsymbol{\theta}}_c$ and $\tilde{\Delta}_c$ are uniformly bounded and converge to a small neighborhood of the origin.